

論文 / 著書情報
Article / Book Information

Title	Submicrosecond laser-filament-assisted corona bursts near a high-voltage electrode
Authors	Kiyohiro Sugiyama, Takashi Fujii, Megumu Miki, Alexei Zhidkov, Masato Yamaguchi, Eiki Hotta, Koshichi Nemoto
Citation	Physics of Plasmas, Vol. 17, 043108,
Pub. date	2010, 4
URL	http://scitation.aip.org/content/aip/journal/pop
Copyright	Copyright (c) 2010 American Institute of Physics

Submicrosecond laser-filament-assisted corona bursts near a high-voltage electrode

Kiyohiro Sugiyama,¹ Takashi Fujii,^{2,a)} Megumu Miki,² Alexei Zhidkov,² Masato Yamaguchi,¹ Eiki Hotta,¹ and Koshichi Nemoto^{1,2}

¹*Department of Energy Sciences, Interdisciplinary Graduate School of Science and Engineering, Tokyo Institute of Technology, 4259 Nagatsuta-cho, Midori-ku, Yokohama-shi, Kanagawa 226-8502, Japan*

²*Electric Power Engineering Research Laboratory, Central Research Institute of Electric Power Industry, 2-6-1 Nagasaka, Yokosuka, Kanagawa 240-0196, Japan*

(Received 3 December 2009; accepted 7 January 2010; published online 19 April 2010)

Long, about a half of microsecond, nonuniform corona UV burst is observed after a femtosecond-laser-filament plasma appears nearby an electrode biased (positively or negatively) slightly higher than the corona discharge threshold and well-isolated from the natural streamer discharge. A bright UV emission area moving outwards, over a 20 cm distance, with the velocity of 0.6% of the speed of light and tearing from the filament plasma in the case of the negative voltage is observed. In the case of positive voltage, a bright, bouncing UV cone is formed at around 4 cm far from the filaments exposing the appearance of a leader. Both phenomena could be explained upon supposing the formation of runaway electrons in the vicinity of the filament plasma and electrode. © 2010 American Institute of Physics. [doi:10.1063/1.3299389]

I. INTRODUCTION

Recently, the laser-filament plasma^{1–17} in a strong external electric field has attracted interest both in the physics of streamer discharges^{18,19} and in various applications such as the discharge triggering,^{20–24} the generation of terahertz radiation,^{25,26} and the measurement of electric fields in atmosphere.²⁷ The electric field measurements with the laser-filament plasma may become an important instrument for geophysical researches and for the implementation of electrical facility protection. However, to make such measurements, practical comprehensive studies of the kinetics and dynamics of the laser-filament plasma in external fields of various configurations is necessary.

Recently, several groups have already reported on experiments with laser-filament plasma in an external field. However, they have mostly focused on the femtosecond-pulse-laser-triggered discharges^{20–24} trying to reduce the breakdown voltage, which has been successfully done. Moreover, the use of laser-induced filament plasma (LFP) has resulted in a considerable lowering of the breakdown voltage and appearance of the fast mode discharges.²³ In the experiments, the dynamics of LFP before the breakdown has not been studied. An interesting phenomenon has been found in pioneering experiment²⁶ on the terahertz radiation of LFP: the intensity of the radiation is very sensitive to the external field strength. The UV radiation of LFP has been also found very sensitive to external field strength:²⁷ it increases nonlinearly with the applied voltage. The measurements in Ref. 27 have been performed for the small size electrode inducing the strong corona. The corona may result in the LFP dynamics and radiation and vice versa.

The field dependency of UV emission may become a

basis for the remote field measurements in the atmosphere and at industrial objects. However, there are various effects which can also result in the LFP emission such as the secondary emission, strong corona, runaway electrons, and so on and, therefore, can change the emission dependency on the field strength. The LFP, itself, may also affect the field distribution in the vicinity of measurements. To make a practical tool, we have to prove the conformity between the emission signal and the external field strength and the ability to maintain it. Detailed studies of LFP behavior in the external fields of different configurations are necessary to understand whether such measurement can be calibrated or can provide only the relative field measurements.

The parameters of LFP such as the electron density and temperature strongly depend on the energy of laser pulses and focusing conditions. Typically, a femtosecond-laser pulse with energy of 20–200 mJ creates in air the LFP with electron density of 10^{16} – 10^{18} cm⁻³ and diameter of $D \sim 0.1$ – 1 mm (Refs. 1–3 and 11) due to the nonlinear Kerr self-focusing and tunnel and/or multiphoton ionization.²⁸ The laser filament has been reported to appear in the atmosphere up to several km from the laser sources.^{6,24} A comprehensive analysis of the laser-filament dynamics in air can be found in Refs. 7. The LFP is not a conventional discharge plasma or laser-breakdown plasma. Even in a strong electric field, LFP is cold and the dissociation recombination reduces the LFP electron density quickly: $N_e = N_{e0} / [1 + \beta N_{e0} t]$, where $\beta \sim 2 \times 10^{-7}$ cm³/s (Refs. 19 and 29) and N_{e0} is the initial electron density in the filament. At $t \leq (\beta N_{e0})^{-1} \sim (5\text{--}500 \text{ ps})$, the LFP is dense, the Debye radius is smaller than a plasma size; electrons do not attach to oxygen molecules. (In this regime, the LFP acquires and maintains a minimal potential in its vicinity.) At $t > (\beta N_{e0})^{-1}$, the electron density loses the information on the initial value. For tens of nanoseconds, the electron density may exceed a “critical” electron density,

^{a)} Author to whom correspondence should be addressed. Electronic mail: fujii@criepi.denken.or.jp.

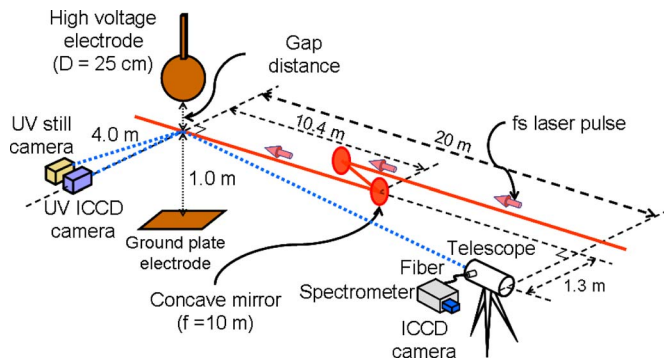


FIG. 1. (Color online) Experimental setup.

$\sim 5 \times 10^{14} \text{ cm}^{-3}$,²³ at which the electron attachment to molecules becomes dominant and the density of negative ions rapidly grows. In this range, discharge between the electrode and LFP, electrons avalanches and streamers heat up plasma and change filament plasma dynamics.

In this paper, we study the dynamics of UV emission from LFP with high spatial and temporal resolution when the electric field at an electrode surface only slightly exceeds the corona discharge threshold of $\sim 30 \text{ kV/cm}$. Both polarities are examined. In contrast to our previous measurements in the strong corona condition,²⁷ we observe long and intense corona bursts and formation of hot, long living plasma structures. The bursts parameters are very sensitive to the LFP position and voltage applied. We scrupulously analyze the burst dynamics to show that it requires the preionizers such as runaway electrons or runaway electrons induced x rays.

II. EXPERIMENTAL SETUP

The scheme of the experimental setup is shown in Fig. 1. A Ti:sapphire laser system (Thales Laser; Alpha 10/US-20TW) was used for producing LFP. The Ti:sapphire laser pulses ($\lambda = 800 \text{ nm}$, $\tau = 50 \text{ fs}$, energy = 84 mJ) with initial diameter of about 50 mm were focused by a concave mirror of 10 m focal length. A negative or positive high voltage was applied on a spherical high-voltage electrode (HVE) with a 250 mm diameter placed at the distance of 10.4 m from the focusing mirror and at least 1 m far from any grounded surface to avoid any effect on laser-induced discharge. A high voltage was varied between 0 and +400 kV or -400 kV. The optical axis of the laser pulse was set at a height of 1.1 m above the floor and 5, 6.8, or 28 mm from the HVE.

The fluorescence of LFP was collected by a telescope with a diameter of 152 mm located 20 m far from the HVE and 1.3 m from the laser axis. The telescope measured plasma over a range of 0.7 m by centering on the bottom of HVE. The fluorescence was detected by a spectrometer (Roper Scientific; SP-2358-P) and by an intensified charge coupled device (ICCD) camera (Roper Scientific; PI-MAX: 1K-UV-MgF2). The gate width and delay time of the ICCD camera were set at each measurement. UV images of LFP were taken by another ICCD camera (Roper Scientific; PI-MAX1K-UniGen) with an UV lens (UV-Nikkor 105 mm F4.5) and a filter (blocking: 400–800 nm) placed at 4 m from HVE perpendicularly to laser axis. (This result was called as

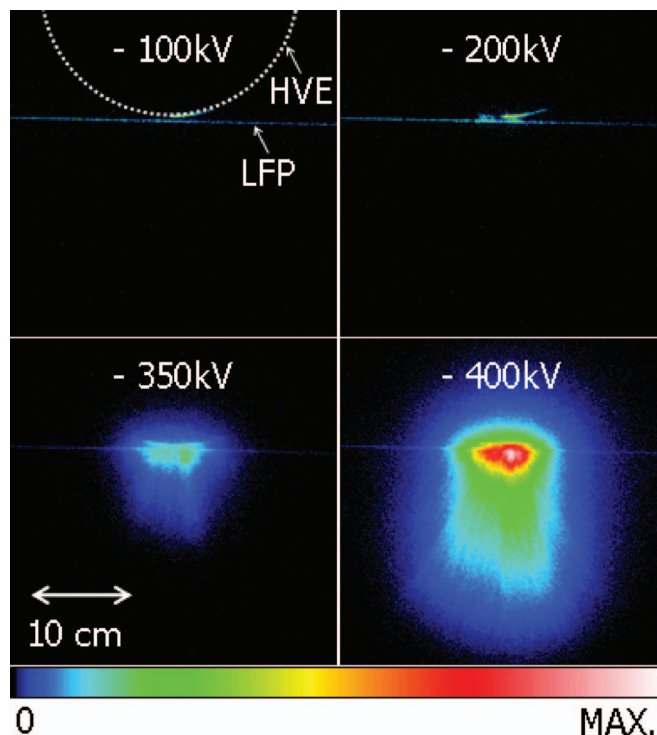


FIG. 2. (Color) UV-ICCD images of the negative corona induced by LFP positioned at 5 mm from the HVE surface at several applied voltages from -100 to -400 kV. The gate width, delay time, and gain of the ICCD camera are 500 μs , 0 s and 250, respectively. The maximal values of color bar are 2000 for -100/-200 kV and 40 000 for -350/-400 kV.

“UV-ICCD image.”) Slightly beside the UV-ICCD camera, a still camera with the UV lens and the filter was set with a film (Kodak; T-MAX P3200). (This result was called as “UV-still image.”) The exposure time of all UV-still images was set at about 10 s that corresponded to accumulate of 100 laser pulses, for which the UV-ICCD images and the spectroscopic data were accumulated. The triggers of the both ICCD cameras were synchronized with the laser pulses. Trigger signal of the spectroscopic measurement has no jitter because the trigger signal was generated by the laser pulse detected by photodiode. On the other hand, the trigger signal for UV-ICCD camera had a $\pm 10 \text{ ns}$ jitter. The delay was defined to be zero when the fluorescence signal at 337.1 nm or the UV image of filament plasma measured with the gate width of 20 ns were strongest without voltage. The fluorescence in the range from 310 to 342 nm was detected.

III. NEGATIVE POLARITY

Images illustrating the voltage dependence and the temporal behavior of the negative corona at different voltages are shown in Figs. 2–4 in the presence of the LFP positioned at 5 or 6.8 mm from the HVE surface. The corona discharges are caused by the LFP already at $U = -200 \text{ kV}$, and become stronger at the higher applied voltages up to -400 kV. Visibly, there was no corona discharge in the absence of the LFP at any voltage applied up to -400 kV. The LFP-induced corona discharges exhibit a complicated dynamics and spatial structure.

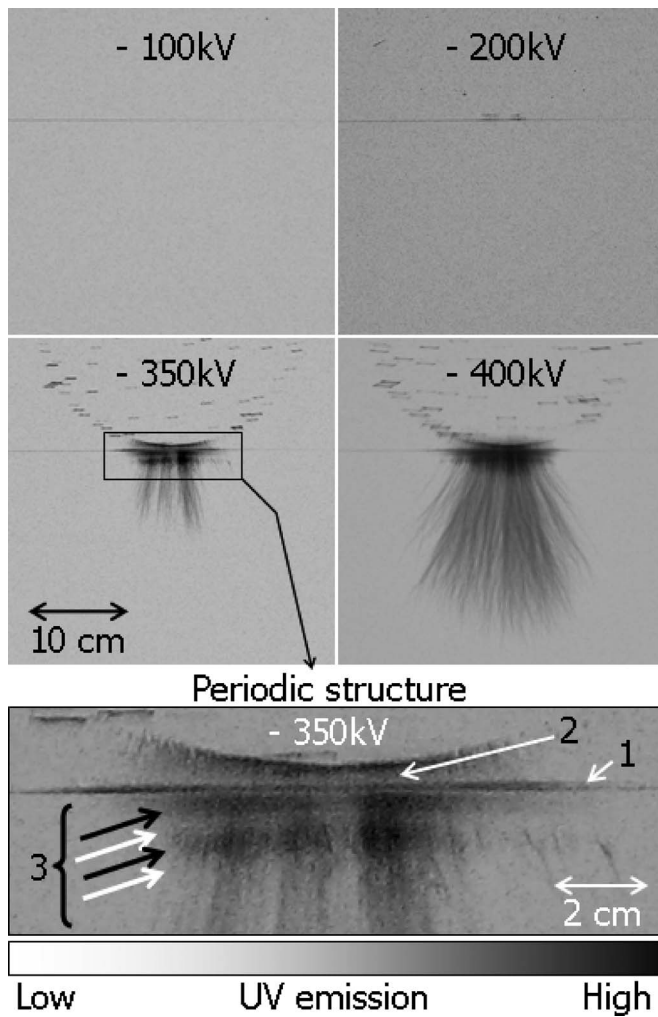


FIG. 3. UV-still images of the negative corona induced by LFP positioned at 5 mm from the HVE surface at several applied voltages from -100 to -400 kV. Each number in the figure showing periodic structure means as follows; 1: LFP radiation, 2: discharge between LFP and HVE, 3: periodic radiation (black and white arrows show bright and dark layers, respectively).

In the conventional negative corona, the Townsend mechanism is known to be responsible for corona discharge with the well-known Paschen condition:

$$\int_{R_0}^{R_{\text{cor}}} [\alpha(E/p) - a(E/p)] dl = \ln(1 + \gamma^{-1}), \quad (1)$$

where α and a are the ionization and attachment coefficients,^{18,19} and γ is the coefficient for a secondary electron emission from the electrode surface at $x=R_0$ (electrode surface); $R_{\text{cor}}-R_0$ is the corona length. In the first sight, if the LFP appears at a distance greater than R_{cor} there is no essential effect on the corona: the filament electrons move outwards, the polarization field rapidly decreases from the filament as $(D/x)^2$ with D the filament radius (~ 0.05 cm). The recombination of the LFP is so rapid that the ions from the plasma cannot reach the electrode to cause the secondary emission: ion mobility is about $\mu=2.1$ cm²/V s (Ref. 19) and the velocity is about 10^5 cm/s at $E\sim 50$ kV/cm and is surely too low for that: the process ceases in 1 μ s as shown below. However, the LFP may affect the corona discharge

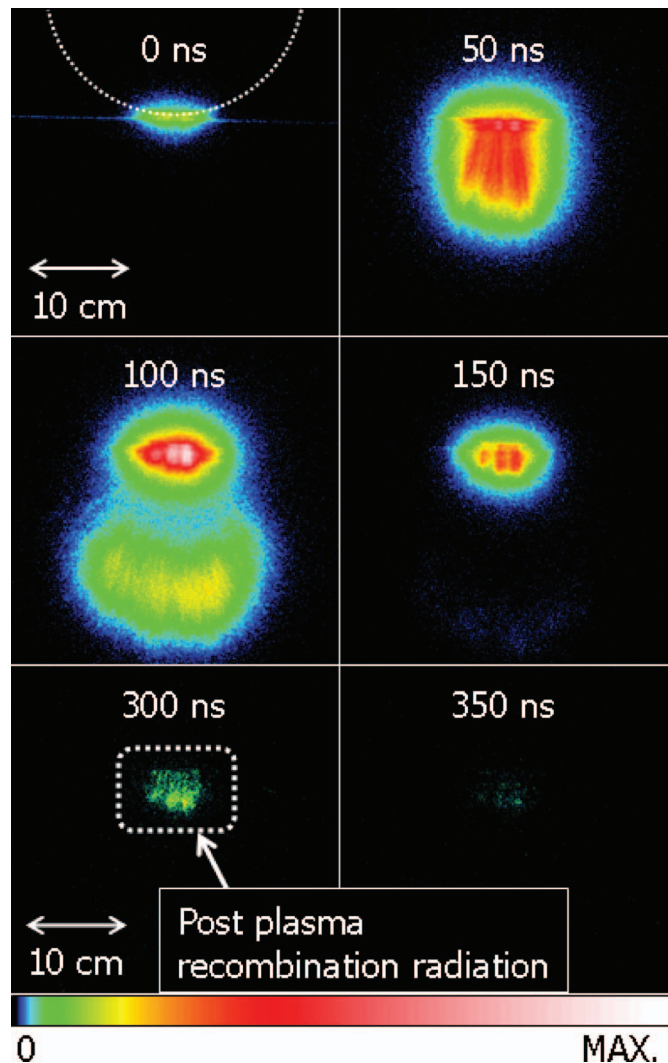


FIG. 4. (Color) UV-ICCD images of the negative corona induced by LFP positioned at 6.8 mm from the HVE surface with the applied voltage of -400 kV at several gate delay times of the ICCD camera from 0 to 350 ns. The maximal values of color bar are 25 000 for 0/150 ns and 2500 for 300/350 ns. The gate width and gain of the ICCD camera are 50 ns and 250, respectively.

via the UV flash, which appears just after the creation of LFP and the consequent electron emission from the electrode. The latter assists the discharge developing between the LFP and the electrode.

Assuming that the electrode electric field does not change much along the LFP in the beginning, one can get the filament field as ~ 60 kV/cm in the experimental conditions using the conventional estimation: $E_f = -\Lambda U_0 \cdot R_0 / R_f^2$, where U_0 is the electrode potential, R_f is the filament position from the center of the electrode, and Λ is the geometrical field gain: for a cylindrical filament $\Lambda=2$. In the absence of inelastic collisions, the LFP electrons would have acquired the average energy, $\bar{\epsilon} \sim \sqrt{M/3m}(eEl)$, with l as the electron free-path and M as the ion mass. For the field in the experiment, this value is about 1 keV. Therefore, at the experimental condition an LFP electron is accelerated and loses its energy for the ionization and excitation till it forms a negative ion in reaction: $O_2 + e \rightarrow O^- + O$ ($\epsilon_{\text{max}} \sim 8$ eV). Then the strong ra-

diation ceases. The intensity of UV flash depends on the field strength²⁷ and plays an important role in the LFP dynamics. The initial UV burst is less than 20% of the maximum emission intensity, as will be shown later.

The UV radiation from the LFP may initiate the electron emission from the electrode. This results in the rapid discharge between the LFP, becoming a virtual anode, and the cathode. This can be seen in Figs. 2–4. If the breakdown appears swiftly, the electron density in LFP is high and the LFP acquires the cathode potential because its capacity is much lower than that of the cathode. As a result, the field at the LFP surface drastically changes: $E_f = -U_0/D$. Since $D \sim 200 \mu\text{m}$, the field may become very high, $\sim 10 \text{ MV/cm}$. Apparently the real field is smaller because the electron density in LFP decreased so rapidly that the LFP cannot maintain the whole electrode potential. (Assuming the streamer type of this discharge and setting the streamer velocity about $\sim 10^8 \text{ cm/s}$, one can get that the time for LFP to acquire the potential is 5 ns for the 5 mm distance between the LFP and electrode.) Nevertheless, such a field is strong enough to provoke the streamer developing outward from the LFP and, probably, cause the electron runaway (see Sec. V). The appearance of the strong field must have a trace: a periodic structure of UV emission beneath the LFP, as clearly seen in Fig. 3, for the UV image at -350 kV . In the strong electric field, the electrons of LFP are accelerated, generating the strong UV emission and losing their energy in the excitation, ionization, and dissociative attachment processes. The periodic structure lining out the LFP consists of dark layers (low UV emission), where the electrons are accelerated by the field, and bright layers (high UV emission), where the electrons lose their energy in inelastic atomic processes. This complex structure of UV emission can be seen in Figs. 2 and 3 for the applied voltage $U_0 = -350 \text{ kV}$ and $U_0 = -400 \text{ kV}$ both in UV-still images and in UV-ICCD images.

Dynamics of the corona discharge in the case of $U_0 = -400 \text{ kV}$ is given in Fig. 4. One can see the two distinct regions. First of all, the discharge is very anisotropic: its length ($\sim 25 \text{ cm}$) exceeds the width by ~ 2.0 times. The field, due to the large electrode diameter of 25 cm, decreases to 4 kV/cm at $L \sim 25 \text{ cm}$, which is about ten times less than the threshold electric field for the positive effective ionization factor. Such a long length of plasma in the area, where $\alpha(E/p) - a(E/p) \leq 0$, cannot be explained by the conventional scenario of the negative streamer discharge in neutral air. The estimation using the electric balance equation and the initial electron density of filament $N_e = 10^{17} \text{ cm}^{-3}$ shows that electrons vanish at the distance of about a few centimeters. On the other hand, the ionization region reached to this place. In most of the UV emission region, except near the HVE, we have $(\alpha - a) < 0$, if ignoring the preionized plasma, which contradicts the appearance of the long ionization region. However, so long preionized area assumes the ionizers such as hard x rays or/and energetic electrons. Figure 5 shows the temporal and spatial evolution of UV emission at the axis perpendicular to the laser filament through the center of the HVE obtained from the results shown in Fig. 4. As shown in Fig. 5, the UV emission spreads over 200 mm far from the electrode for about 100 ns. On the other hand, the

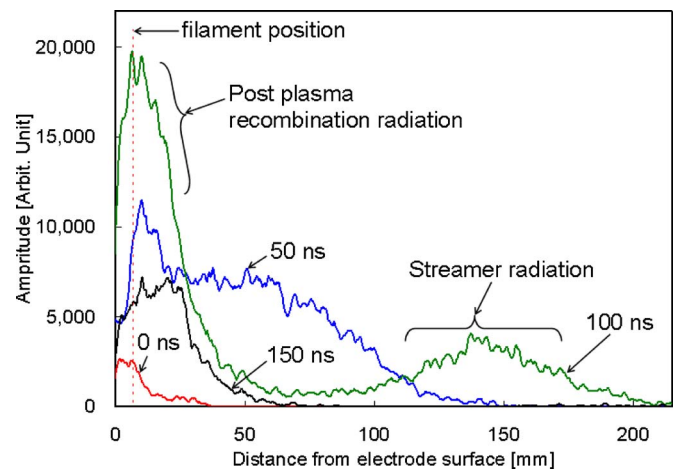


FIG. 5. (Color online) Temporal and spatial evolution of UV emission in the cross section perpendicular to the laser filament obtained from the UV-ICCD images shown in Fig. 4. The cross section is vertically through the point on filament that is the closest to the electrode surface.

emission at the filament position continuously increased in the first 100 ns. Figure 6 shows the evolution of the UV emission front, the point at 10% of the maximum intensity, obtained from the results shown in Fig. 5. From Fig. 6, the velocity of the UV emission front was estimated to be 0.6% of the speed of light. As seen from Figs. 4 and 5, the strong streamer radiation at a distance quite far from the electrode lasted for $\sim 150 \text{ ns}$, and the postplasma recombination radiation emitted for $\sim 0.5 \mu\text{s}$. Such a long emission can be produced by a hot plasma, in our case the best fitting gives $T_e \sim 10 \text{ eV}$ and $N_e \sim 10^{15} \text{ cm}^{-3}$ (from local kinetic simulations¹⁹). This velocity agrees well with the velocity of the streamers.¹⁸ The two distinguished regions may just reflect (i) the radiation of the streamer heads, far from the electrode and (ii) the radiation of recombining LFP.

We performed the same measurements with the LFP positioned at 28 mm from the electrode as well. The voltage dependence and the temporal behavior of the negative corona in the presence of the LFP at 28 mm from the electrode are shown in Figs. 7–9. There is no essential difference in the behavior with the voltage among the 5, 6.8, and 28 mm distance except the brightness of the initial UV burst from

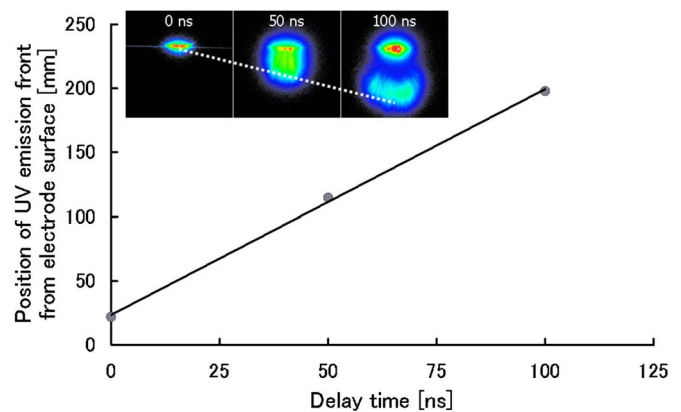


FIG. 6. (Color online) Evolution of the position of the UV emission front obtained from the results shown in Fig. 5.

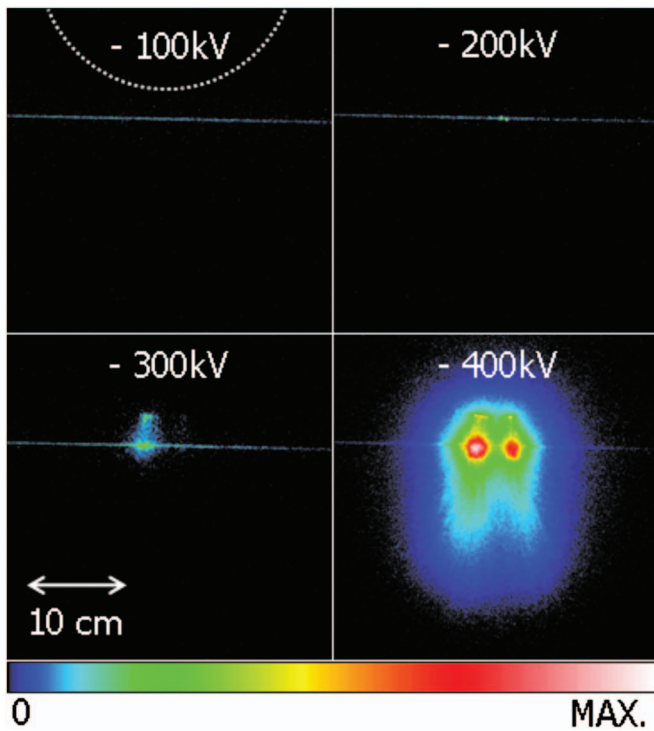


FIG. 7. (Color) UV-ICCD images of the negative corona induced by LFP positioned at 28 mm from the HVE surface at several applied voltages from -100 to -400 kV. The gate width, delay time and gain of the ICCD camera are $500 \mu\text{s}$, 0 s and 250 , respectively. The maximal values of color bar are 2000 for $-100/-300$ kV and $30\,000$ for -400 kV.

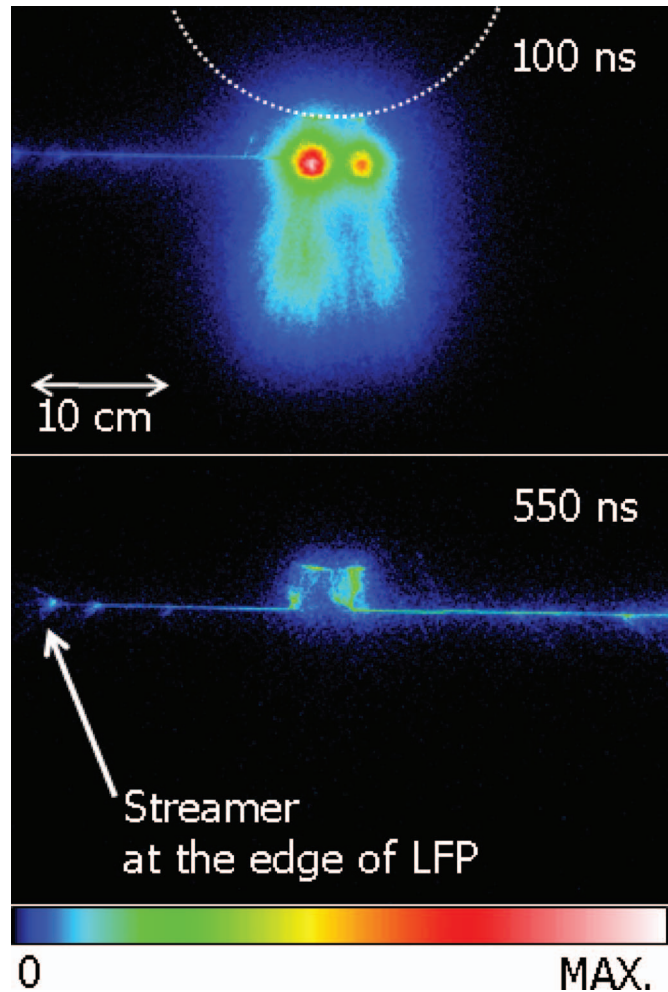


FIG. 9. (Color) UV-ICCD images of the negative corona induced by LFP positioned at 28 mm from the HVE surface with the applied voltage of -400 kV at gate delay times of the ICCD camera of 100 and 550 ns. The maximal values of color bar are $40\,000$ for 100 ns and $10\,000$ for 550 ns. The gate widths of the ICCD camera are 50 and $100 \mu\text{s}$ for the gate delay time of 100 and 550 ns, respectively, with the gain of 250 .

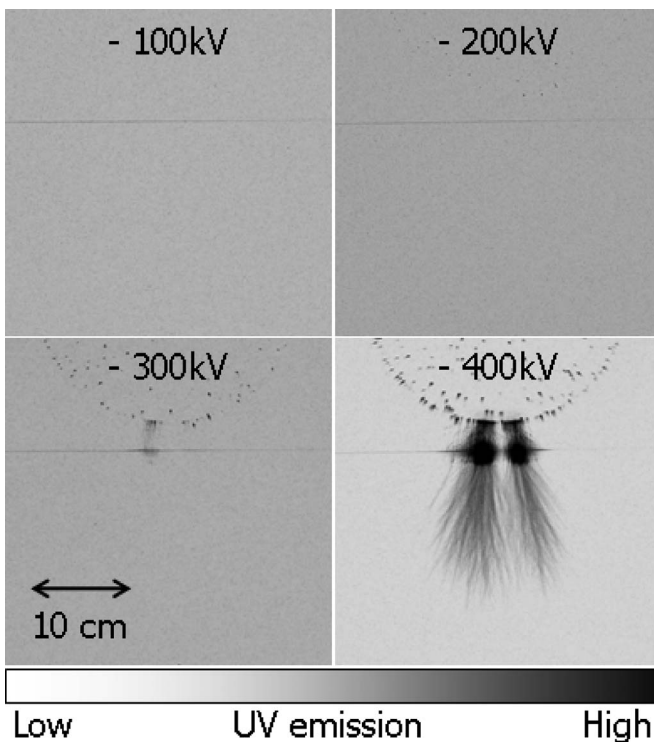


FIG. 8. UV-still images of the negative corona induced by LFP positioned at 28 mm from the HVE surface at several applied voltages from -100 to -400 kV.

LFP irradiating the gap and the electrode surface, as seen in Figs. 7 and 8. The clearly seen streamers at the edge of LFP, as seen in Fig. 9, prove that the LFP has the electrode potential.

The voltage dependence and temporal evolution of the UV spectra in the vicinity of LFP detected by the telescope is presented in Fig. 10 for the 313.6, 315.9, and 337.1 nm nitrogen lines ($\text{N}_2: \text{C}^3\Pi_u \rightarrow \text{N}_2: \text{B}^3\Pi_g$). The temporal evolution of the peak signal height of N_2 fluorescence corresponds well to that of the UV emission in the vicinity of LFP shown in Fig. 5. One can see the strong dependence of the UV spectra on the external voltage. These UV spectra can be used for the electric field diagnosis: it reflects the real field near the LFP.

IV. POSITIVE POLARITY

We also tested the positive corona, as shown in Figs. 11–13, in the presence of the LFP positioned at 5 mm from the HVE surface. Again, in the absence of the LFP, we observe no corona discharge. The LFP drastically changes the

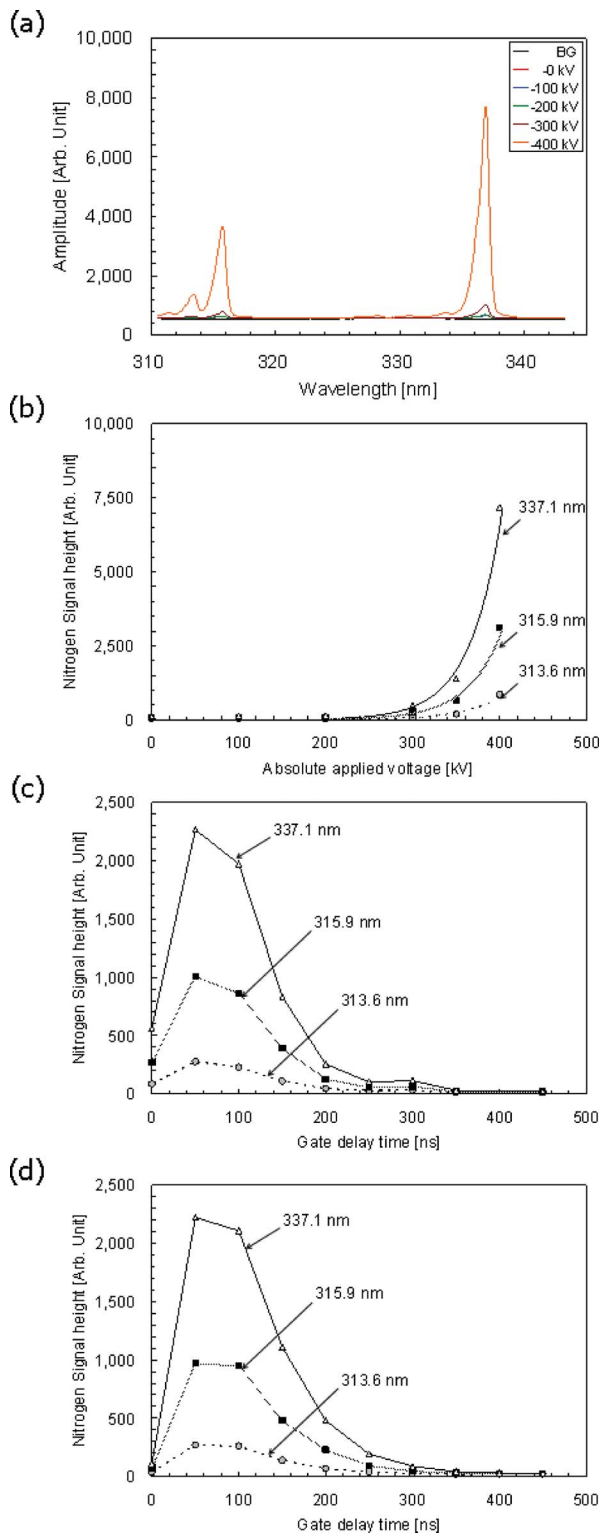


FIG. 10. (Color online) Fluorescence spectra of N₂ molecules and peak signal height of the N₂ fluorescence for the wavelengths of 313.6, 315.9, and 337.1 nm in the vicinity of the HVE and filament when the optical axis of the laser beam is set at [(a)–(c)] 5 mm and (d) 28 mm from the HVE surface for the negative polarity. (a) Fluorescence spectra of N₂ molecules at several applied voltages and background spectra (shown as BG) taken at a voltage of -400 kV without the LFP, (b) peak signal height of the N₂ fluorescence over background spectra as a function of applied voltage, and [(c) and (d)] peak signal height of the N₂ fluorescence over background spectra as a function of the gate delay time of the ICCD camera with the applied voltage of -400 kV. The gate width and delay time of the ICCD camera for the experiments shown in (a) and (b) are 500 ns and 0 s, respectively. The gate width of the ICCD camera for the experiments shown in (c) and (d) is 50 ns.

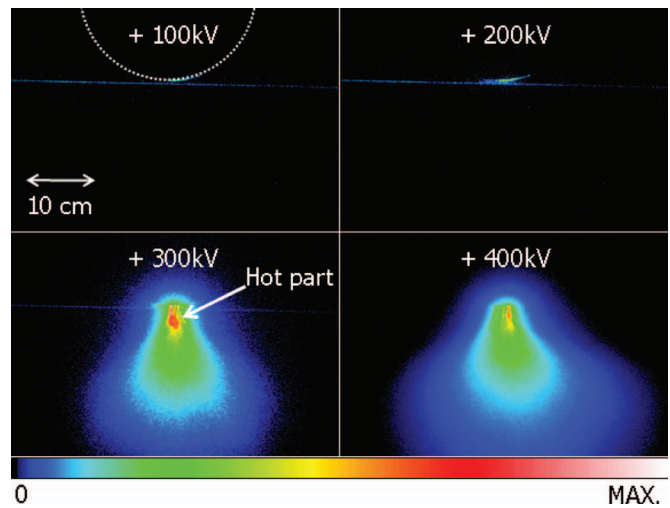


FIG. 11. (Color) UV-ICCD images of the positive corona induced by LFP positioned at 5 mm from the HVE surface at several applied voltages from 100 to 400 kV. The gate width and delay time of the ICCD camera are 500 μ s and 0 s, respectively. The gain of the ICCD camera is 250 for 100/300 kV and 50 for 400 kV. The maximal values of color bar are 3000 for 100/200 kV and 30 000 for 300/400 kV.

corona dynamics. In the experiments, the irradiation of a laser pulse was followed by a loud sound as if after a lightning revealing the formation of hot plasma in the positive corona with LFP and accompanying acoustic waves.

In the figures, one can see a scenario which is expectedly different from that for the negative streamer. The Townsend mechanism does not work in the positive corona.^{18,19} In this case, one can expect a stronger effect of the LFP because the electrons from the plasma could reach the electrode: the necessary time is about 20 ns since electron mean velocity in air at the field strength $E \sim 30$ kV/cm is not high, about 2×10^7 cm/s.¹⁹ However, the electron evacuation must be rapidly ceased when $U_0 R_0 / R^2 \sim U_f / D$ where R is a distance between the center of the filament and the filament, and U_f is the LFP potential; this process results in the strong initial UV emission from LFP. In the case of the positive polarity UV emission cannot provoke a discharge between the LFP and electrode; the UV emission may only preionize air to stimulate the positive streamers, as seen in Fig. 12, where the snapshots of the positive corona are presented.

This scenario is well proved by the plasma dynamics illustrated by Figs. 13 and 14. In the figures, the temporal evolution of UV emission in the space is shown, though the integration time is large: 50 μ s. Again, one can see two very distinguished regions: the vicinity of the LFP and the area around 4 cm far from the filament and the electrode. As well as the negative corona, the UV emission of LFP rapidly decreases in 200 ns, while the UV emission at a far distance, as seen in Fig. 14, lasts for more than 0.5–0.6 μ s. Again, such a long emission is possible only from hot air plasma: $T_e \sim 10$ eV and $N_e \sim 10^{15}$ cm⁻³.¹⁹ This bright distant area is quite big: $(\sim 5-7) \times \sim 3$ cm²; the brightest area is far from the filament and the electrode, its position does not change during the discharge. This region, therefore, exhibits all characteristics of a leader. Numerous streamers start from the

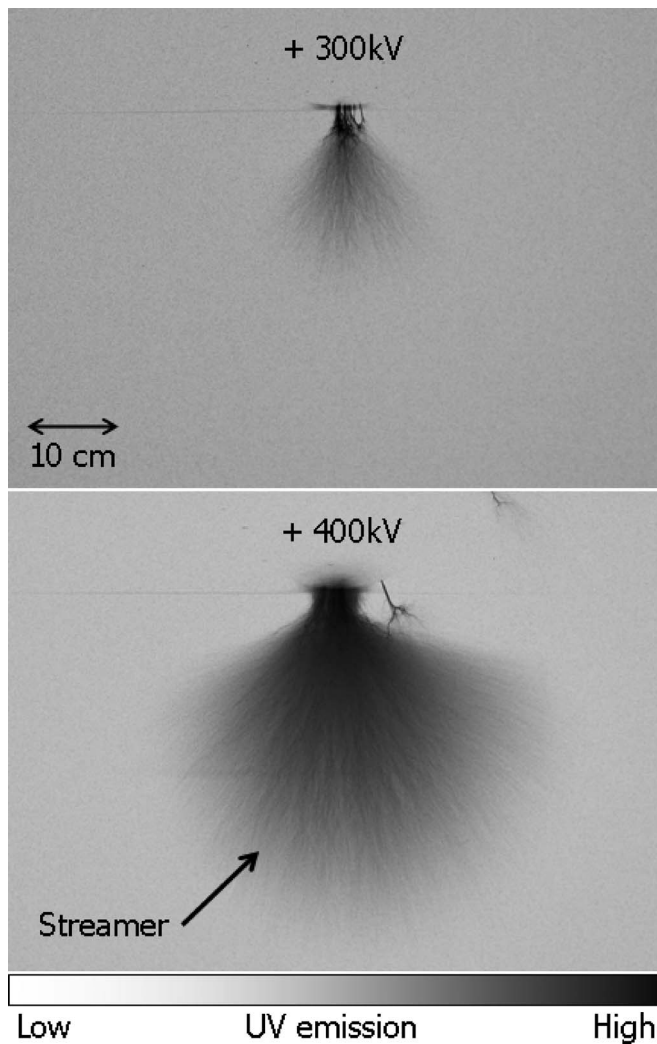


FIG. 12. UV-still images of the positive corona induced by LFP positioned at 5 mm from the HVE surface at applied voltages of 300 and 400 kV.

leader head and propagate downwards in the distance about 30–50 cm heating the leader head.

Appearance of leaders provoked by the LFP is difficult to explain by the streamer developing in the neutral air without the seeding electrons. In fact, to make such a long and thick leader, a long preionized plasma channel seems to be necessary. However, the free-paths of the ionizing UV radiation are too short (< 1 mm) to make such a channel. Only x-ray emission could make such preionization. However in the case of positive corona the electrons may run away only toward the electrode. In general, it might be a source of x rays.

The voltage dependence and temporal evolution of the UV spectra in the vicinity of LFP detected by the telescope is presented in Fig. 15. The dynamics of the UV spectra is very similar to that for the negative potential, though the characteristics of the laser-induced corona discharges are much different, and can be utilized for the electric field diagnosis.

V. HYPOTHESIS OF RUNAWAY ELECTRONS

We summarize all features observed in the experiments in Fig. 16 where the stages of the LFP-induced corona bursts

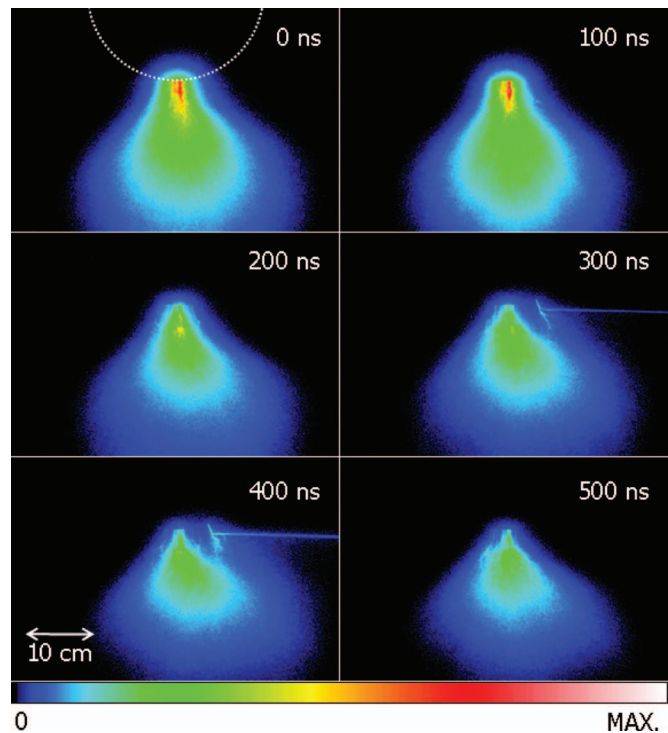


FIG. 13. (Color) UV-ICCD images of the positive corona induced by LFP positioned at 5 mm from the HVE surface with the applied voltage of 400 kV at several gate delay times of the ICCD camera from 0 to 500 ns. The maximal value of color bar is 10 000. The gate width and gain of the ICCD camera are 50 μ s and 50, respectively.

are presented. In the first stage, the filament formation proceeds similarly for either polarity because the corona is very weak. In the second stage, we observe the formation of the streamer discharge between the filament and the electrode. For the negative polarity, it is provoked by the initial UV burst from the filament in the external field, while for the positive polarity, it is the conventional streamer discharge with the seeding electrons which come from the filament. In the third stage, the filament acquires the electrode potential and the long, intensive UV burst produced by the leader and

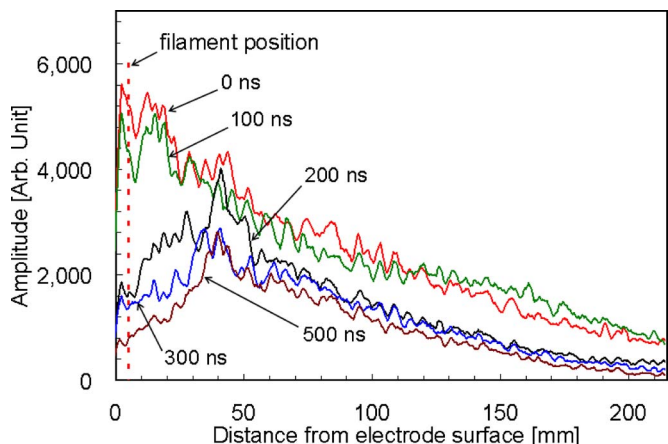


FIG. 14. (Color online) Temporal and spatial evolution of UV emission at the cross section perpendicular to the laser filament obtained from the UV-ICCD images shown in Fig. 13. The cross section is vertically through the point on filament that is the closest to the electrode surface.

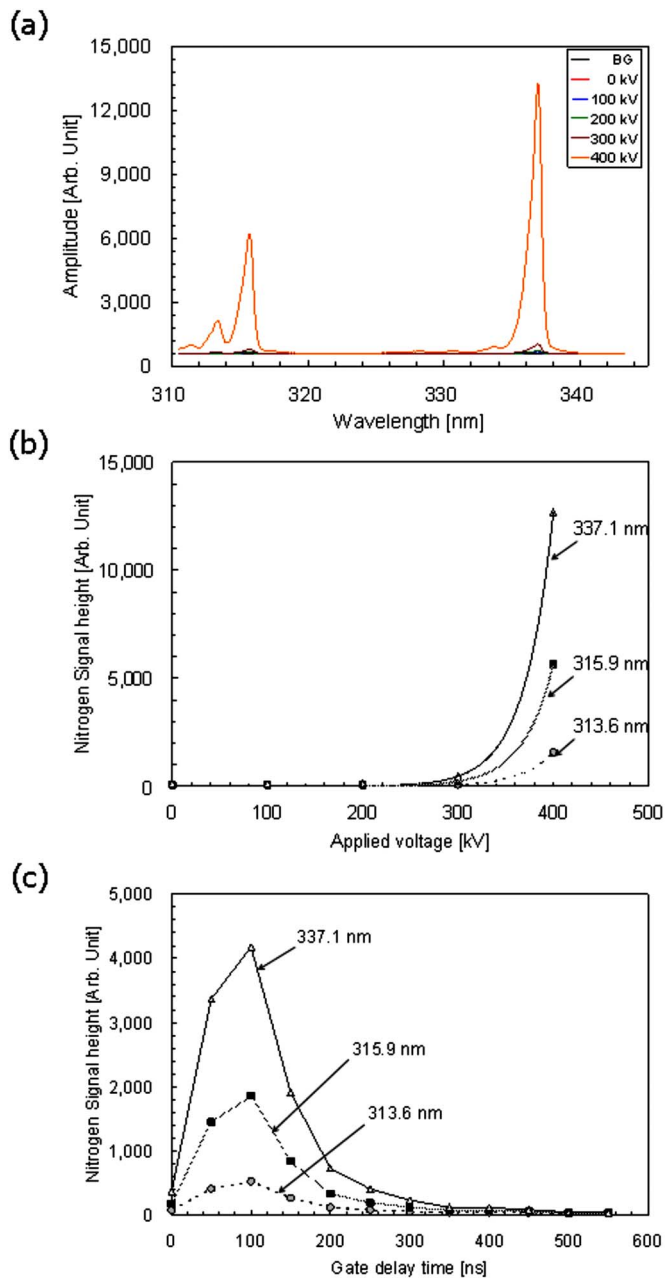


FIG. 15. (Color online) Fluorescence spectra of N₂ molecules and peak signal height of the N₂ fluorescence for the wavelengths of 313.6, 315.9, and 337.1 nm in the vicinity of the HVE and filament when the optical axis of the laser beam was set at 5 mm from the HVE surface for the positive polarity. (a) Fluorescence spectra of N₂ molecules at several applied voltages and background spectra (shown as BG) taken at a voltage of 400 kV without the LFP, (b) peak signal height of the N₂ fluorescence over background spectra as a function of applied voltage, and (c) peak signal height of the N₂ fluorescence over background spectra as a function of the gate delay time of the ICCD camera with the applied voltage of 400 kV. The gate width and delay time of the ICCD camera for the experiments shown in (a) and (b) are 500 and 0 ns, respectively. The gate width of the ICCD camera for the experiments shown in (c) is 50 ns.

streamers appears. In the last stage, we observe a long recombination of the leader plasma: the filament in the case of the negative polarity and the area ~ 4 cm far from the electrode in the case of the positive polarity. The characteristics of the third part of the corona burst and appearance of the quite hot plasma make us hope that an interesting phenom-

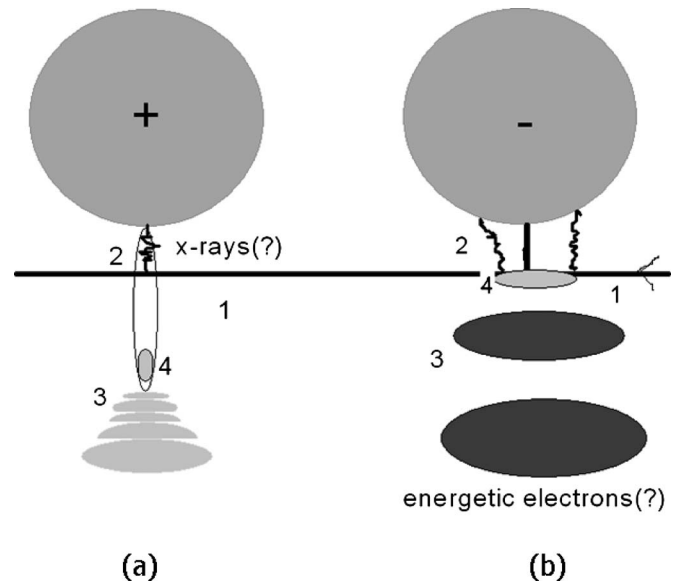


FIG. 16. The scenario of the corona bursts for the positive (a) and the negative (b) polarities. 1—the filament formation; 2—the discharge between the filament and the electrode; 3—the streamer stage; 4—the recombination of the leader part.

enon might appear in the experiment: the runaway electrons.

A discussion on the electron runaway in gas discharges has been started long time ago.³⁰ However, so far, there is no complete physical picture of the process.³¹ Nevertheless, the appearance of runaway electrons in gas discharges including lightning at certain conditions is doubtless.³²

The effect of runaway electrons in gas discharge appears in strong electric field. An electron to runaway has to acquire the kinetic energy from the field greater than the energy it lost by ionization, excitation, and dissociation of air molecules: $eEl > \epsilon_{\text{lost}}$, where $l \sim (\sigma N)^{-1}$ with N as the air density, σ as an effective inelastic cross section, and ϵ_{lost} as an effective energy. Choosing the Lotz ionization cross section: $\sigma_{\text{ion}} = 4 \times 10^{-14} \xi \ln(\epsilon/I) / (\epsilon I)$ cm² (Refs. 19 and 33) (ϵ is an electron energy, I is the ionization potential, and ξ is the number of equivalent electrons) and $\epsilon_{\text{lost}} \sim I$, one can get an estimation for the runaway field strength $E_{\text{RW}} \sim 0.5$ MV/cm for an initially zero-energy electron. The detailed calculation (see Ref. 30 for example) gives for E_{RW} a bit lower value in air, ~ 320 kV/cm. In any rate, such a field is very high; it vanishes shortly due to the corona effects. However, in such a field, all electrons in plasma would run away. Assuming the LFP density $N_f \sim 10^{17}$ cm⁻³, the diameter $D \sim 0.05$ cm, and an effective length of ~ 5 cm, one can get the charge of accelerated electrons $Q \sim 0.2$ mC in air at $E = E_{\text{RW}}$. However, an electron can run away if it has already a high energy. In Fig. 17, the energy required for the runaway in the field of 30 kV/cm produced by the electrode and concentrated by the LFP is shown as a function of the geometry parameter Λ . The electron to be accelerated has to acquire the initial energy of about 0.5–0.9 keV. Generally speaking, it is possible in the electrode-LFP discharge stage before the LFP acquires the electrode potential. The calculation similar to that in Ref. 19 shows that in the field of 30 kV/cm in 5 mm distance approximately 10^{-6} of LFP electron may reach the energy of

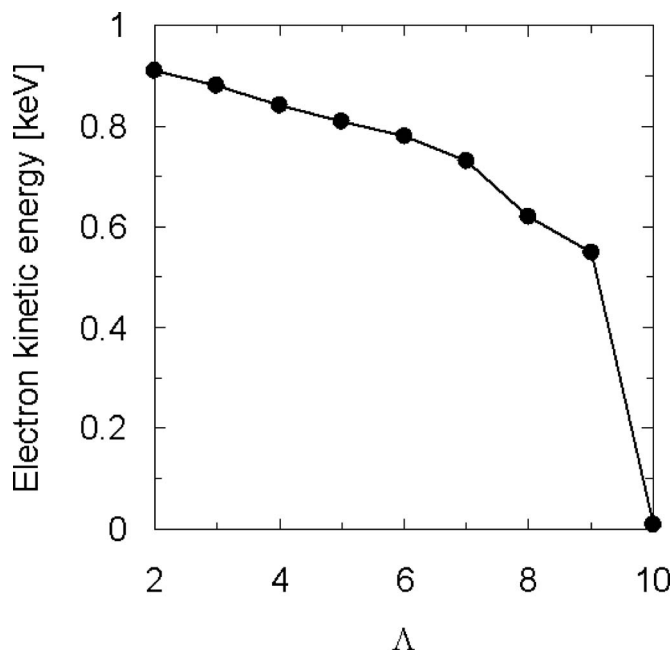


FIG. 17. The energy required for the runaway in the electric field of 30 kV/cm produced by the electrode and concentrated by the LFP as a function of the geometry parameter Δ .

1 keV. Therefore, the charge of accelerated electrons may be about 100 pC.

The appearance of runaway electrons could explain the long corona burst in the case of the negative polarity and its complicated structure as the streamer propagation in air preionized by the runaway electrons that would have the free-path of about 10/20 cm. This effect could also explain the appearance of the long leader in the case of the positive polarity that might be a result of streamer developing in the air preionized by x rays generated by the runaway electrons from the electrode surface.

The complete answer needs x-ray measurements from the LFP-induced corona discharges, which is difficult because of the strong absorption of the x rays with the range of 1–10 keV in air.

VI. CONCLUSION

We have performed the imaging and spectral measurement of UV from laser-filament plasma in an external field of different polarities produced by the spherical electrode with a 25 cm diameter. The field dependency of the UV emission is very similar to that observed in the experiments with the small sphere electrode when the electrode-induced corona affects the LFP-electrode interaction. It is shown to be useful at least for the relative field measurements (detection of field distribution). However, the dynamics of UV emission is very different. Though similar to Ref. 27, the discharge between the LFP and electrode plays the dominant role, we have observed the long (tens of centimeters) positive and negative corona induced by the laser-filament plasma initiated by a femtosecond-laser pulse in the vicinity of an isolated electrode without an initial corona. We have detected the different stages of the corona bursts: the initial UV flash from the

LFP; the UV flash from discharge between the LFP as a virtual electrode and the real electrode; and UV from the streamer discharges and the hot leader plasma.

The corona dynamics is found to depend strongly on the polarity while the initial UV bursts from filament run similarly. At the negative polarity, the LFP-electrode discharge runs for a half-microsecond and the streamer discharge lasts much shorter, ~ 200 ns; at the positive polarity the streamer discharge firming a long, $\sim 5\text{--}7$ cm, and thick, ~ 3 cm, leader lasts for more than $0.6 \mu\text{s}$ and UV emission from the vicinity of filament rapidly decreases in 200 ns.

The spatial structure of the burst is also complicated. For the negative polarity, we have observed the stratified UV emission near the filament and the second UV emission peak 15 cm far from the filament. We attributed the strata to electron drag in the strong electric field formed at the LFP after the LFP-electrode discharge. The second UV peak can be explained either by the streamer developing at the velocity 0.6% of the speed of light at a softer Paschen condition (that, however, cannot be maintained only for a short time, ~ 1 ns), or by the air preionization by runaway electrons formed when the LFP acquires the electrode potential. Since these electrons deposit their energy via ionization at the distance of $\sim 10/20$ cm far from the LFP, the streamer can be lengthened and initiates the bright UV emission far from LFP. The structure of the positive corona burst exhibits the formation of the leader with the hot, $T_e \sim 10$ eV, dense, $N_e \sim 10^{15} \text{ cm}^{-3}$ plasma. This also requires the strong preionization. In the case of the positive corona such a preionization could be produced by x rays generated by runaway electrons from the electrode surface. The free-path of x rays ~ 1 keV in the air is about a few centimeters that length goes well with the size of the leader. If the runaway electrons appearance is true at the condition considered, the LFP may become the unique instrument for emulating the electron runaway appearance in the natural lightning.

¹A. Braun, G. Korn, X. Liu, D. Du, J. Squier, and G. Mourou, *Opt. Lett.* **20**, 73 (1995).

²B. La Fontaine, F. Vidal, Z. Jiang, C. Y. Chien, D. Comtois, A. Desparois, T. W. Johnston, J.-C. Kieffer, and H. Pépin, *Phys. Plasmas* **6**, 1615 (1999).

³H. Yang, J. Zhang, Y. Li, J. Zhang, Y. Li, Z. Chen, H. Teng, Z. Wei, and Z. Sheng, *Phys. Rev. E* **66**, 016406 (2002).

⁴J. Yu, D. Mondelain, J. Kasparian, E. Salmon, S. Geffroy, C. Favre, V. Boutou, and J.-P. Wolf, *Appl. Opt.* **42**, 7117 (2003).

⁵G. Méchain, A. Couairon, M. Franco, B. Prade, and A. Mysyrowicz, *Phys. Rev. Lett.* **93**, 035003 (2004).

⁶M. Rodriguez, R. Bourayou, G. Méjean, J. Kasparian, J. Yu, E. Salmon, A. Scholz, B. Stecklum, J. Eislöffel, U. Laux, A. P. Hatzes, R. Sauerbrey, L. Wöste, and J.-P. Wolf, *Phys. Rev. E* **69**, 036607 (2004).

⁷S. Skupin, L. Bergé, U. Peschel, F. Lederer, G. Méjean, J. Yu, J. Kasparian, E. Salmon, J. P. Wolf, M. Rodriguez, L. Wöste, R. Bourayou, and R. Sauerbrey, *Phys. Rev. E* **70**, 046602 (2004); J. R. Peñano, P. Sprangle, B. Hafizi, A. Ting, D. F. Gordon, and C. A. Kapetanios, *Phys. Plasmas* **11**, 2865 (2004); S. Champeaux and L. Bergé, *Phys. Rev. E* **71**, 046604 (2005).

⁸S. L. Chin, S. A. Hosseini, W. Liu, Q. Luo, F. Théberge, N. Aközbek, A. Becker, V. P. Kandidov, O. G. Kosareva, and H. Schroeder, *Can. J. Phys.* **83**, 863 (2005).

⁹A. Ting, D. F. Gordon, E. Briscoe, J. R. Peñano, and P. Sprangle, *Appl. Opt.* **44**, 1474 (2005); A. Ting, I. Alexeev, D. Gordon, R. Fischer, D. Kaganovich, T. Jones, E. Briscoe, J. Peñano, R. Hubbard, and P. Sprangle, *Phys. Plasmas* **12**, 056705 (2005).

- ¹⁰R. Ackermann, G. Méjean, J. Kasparian, J. Yu, E. Salmon, and J.-P. Wolf, *Opt. Lett.* **31**, 86 (2006).
- ¹¹F. Théberge, W. Liu, P. Tr. Simard, A. Becker, and S. L. Chin, *Phys. Rev. E* **74**, 036406 (2006).
- ¹²L. Bergé, S. Skupin, R. Nuter, J. Kasparian, and J.-P. Wolf, *Rep. Prog. Phys.* **70**, 1633 (2007).
- ¹³A. Couairona and A. Mysyrowicz, *Phys. Rep.* **441**, 47 (2007).
- ¹⁴Y. Chen, F. Théberge, O. Kosareva, N. Panov, V. P. Kandidov, and S. L. Chin, *Opt. Lett.* **32**, 3477 (2007).
- ¹⁵S. Champeaux and L. Bergé, *Phys. Rev. E* **77**, 036406 (2008).
- ¹⁶Y. Ma, X. Lu, T.-t. Xi, Q.-h. Gong, and J. Zhang, *Opt. Express* **16**, 8332 (2008).
- ¹⁷J. Bernhardt, W. Liu, F. Théberge, H. L. Xu, J. F. Daigle, M. Châteauneuf, J. Dubois, and S. L. Chin, *Opt. Commun.* **281**, 1268 (2008).
- ¹⁸L. B. Loeb and J. M. Meek, *The Mechanism of the Electric Spark* (Oxford University, Oxford, 1941).
- ¹⁹Y. P. Raizer, *Gas Discharge Physics* (Springer-Verlag, Berlin, 1991), pp. 60–63.
- ²⁰B. La Fontaine, D. Comtois, C.-Y. Chien, A. Desparois, F. Génin, G. Jarry, T. Johnston, J.-C. Kieffer, F. Martin, R. Mawassi, H. Pépin, F. A. M. Rizk, F. Vidal, C. Potvin, P. Couture, and H. P. Mercure, *J. Appl. Phys.* **88**, 610 (2000).
- ²¹M. Rodriguez, R. Sauerbrey, H. Wille, L. Wöste, T. Fujii, Y.-B. André, A. Mysyrowicz, L. Klingbeil, K. Rethmeier, W. Kalkner, J. Kasparian, E. Salmon, J. Yu, and J.-P. Wolf, *Opt. Lett.* **27**, 772 (2002).
- ²²D. F. Gordon, A. Ting, R. F. Hubbard, E. Briscoe, C. Manka, S. P. Slinker, A. P. Baronavski, H. D. Ladouceur, P. W. Grounds, and P. G. Girardi, *Phys. Plasmas* **10**, 4530 (2003).
- ²³T. Fujii, M. Miki, N. Goto, A. Zhidkov, T. Fukuchi, Y. Oishi, and K. Nemoto, *Phys. Plasmas* **15**, 013107 (2008).
- ²⁴J. Kasparian, R. Ackermann, Y.-B. André, G. Méchain, G. Méjean, B. Prade, P. Rohwetter, E. Salmon, K. Stelmasczyk, J. Yu, A. Mysyrowicz, R. Sauerbrey, L. Wöste, and J.-P. Wolf, *Opt. Express* **16**, 5757 (2008).
- ²⁵S. Tzortzakis, G. Méchain, G. Patalano, Y.-B. André, B. Prade, M. Franco, and A. Mysyrowicz, *Opt. Lett.* **27**, 1944 (2002).
- ²⁶A. Houard, Y. Liu, B. Prade, V. T. Tikhonchuk, and A. Mysyrowicz, *Phys. Rev. Lett.* **100**, 255006 (2008).
- ²⁷K. Sugiyama, T. Fujii, M. Miki, M. Yamaguchi, A. Zhidkov, E. Hotta, and K. Nemoto, *Opt. Lett.* **34**, 2964 (2009).
- ²⁸S. L. Chin, in *Advances in Multi-Photon Processes and Spectroscopy*, edited by S. H. Lin, A. A. Villaeys, and Y. Fujimura (World Scientific, Singapore, 2004), pp. 249–272.
- ²⁹F. J. Mehr and M. A. Biondi, *Phys. Rev.* **181**, 264 (1969).
- ³⁰A. V. Gurevich, G. M. Milikh, and R. A. Roussel-Dupre, *Phys. Lett. A* **165**, 463 (1992); R. A. Roussel-Dupré, A. V. Gurevich, T. Tunnell, and G. M. Milikh, *Phys. Rev. E* **49**, 2257 (1994); L. P. Babich, T. V. Loiko, and V. A. Tsukerman, *Sov. Phys. Usp.* **33**, 521 (1990).
- ³¹V. F. Tarasenko and S. I. Yakovlenko, *Phys. Usp.* **47**, 887 (2004); V. F. Tarasenko, *Appl. Phys. Lett.* **88**, 081501 (2006); L. P. Babich, *Phys. Usp.* **48**, 1015 (2005).
- ³²J. R. Dwyer, Z. Saleh, H. K. Rassoul, D. Concha, M. Rahman, V. Cooray, J. Jerauld, M. A. Uman, and V. A. Rakov, *J. Geophys. Res.* **113**, D23207 (2008); H. Tsuchiya, T. Enoto, S. Yamada, T. Yuasa, M. Kawaharada, T. Kitaguchi, M. Kokubun, H. Kato, M. Okano, S. Nakamura, and K. Makishima, *Phys. Rev. Lett.* **99**, 165002 (2007); H. Tsuchiya, T. Enoto, T. Torii, K. Nakazawa, T. Yuasa, S. Torii, T. Fukuyama, T. Yamaguchi, H. Kato, M. Okano, M. Takita, and K. Makishima, *ibid.* **102**, 255003 (2009).
- ³³W. Lotz, *Z. Phys.* **206**, 205 (1967); **216**, 241 (1968).